AD-A112 670 PITTSBURGH UNIV PA INST FOR COMPUTATIONAL MATHEMATICS--ETC F/G 20/11
EVOLUTION AND MERGER OF ISOLATED VORTEX STRUCTURES.(U)
OCT 81 E A OVERMAN, N J ZABUSKY N00014-77-C-0520
UNCLASSIFIED ICMA-81-31 NL

END
DATE FILMED
4 82
DTIC

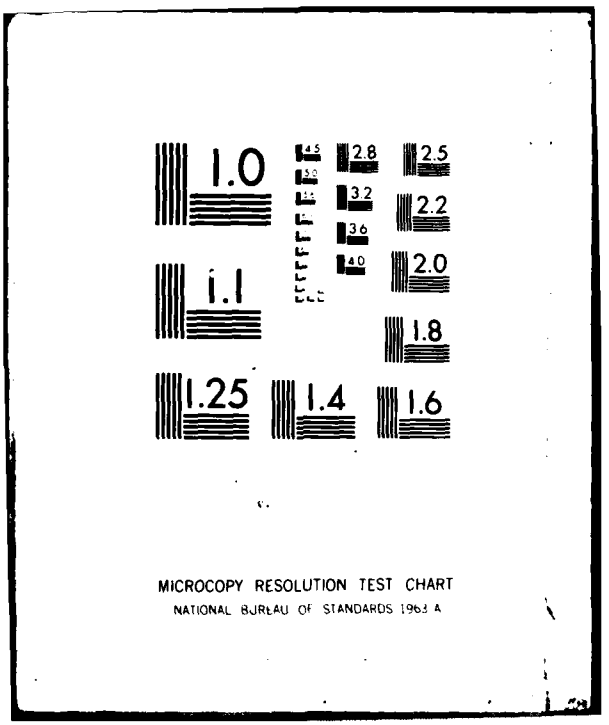
1.0
1.1
1.25
1.4
1.6
1.8
2.0
2.2
2.5
2.8
3.2
3.6
4.0
MICROCOPY RESOLUTION TEST CHART
NATIONAL BUREAU OF STANDARDS 1963 A

AD A112670

REPORT DOCUMENTATION PAGE		READ INSTRUCTIONS BEFORE COMPLETING FORM
1. REPORT NUMBER ICMA 81-31	2. GOVT ACCESSION NO. AD-A112670	3. RECIPIENT'S CATALOG NUMBER
4. TITLE (and Subtitle) Evolution and Merger of Isolated Vortex Structures		5. TYPE OF REPORT & PERIOD COVERED Preprint 6. PERFORMING ORG. REPORT NUMBER
7. AUTHOR(s) E. A. Overman, II and N. J. Zabusky		8. CONTRACT OR GRANT NUMBER(s) N00014-77-C-0520
9. PERFORMING ORGANIZATION NAME AND ADDRESS University of Pittsburgh Department of Mathematics and Statistics Pittsburgh, PA 15260		10. PROGRAM ELEMENT, PROJECT, TASK AREA & WORK UNIT NUMBERS Task No. 062-583
11. CONTROLLING OFFICE NAME AND ADDRESS Fluid Dynamics Program Office of Naval Research Arlington, VA 22217		12. REPORT DATE October, 1981 13. NUMBER OF PAGES 21 pages + tables + 13 figur
14. MONITORING AGENCY NAME & ADDRESS(if different from Controlling Office) Same		15. SECURITY CLASS. (of this report) 15a. DECLASSIFICATION/DOWNGRADING SCHEDULE

16. DISTRIBUTION STATEMENT (of this Report)

Approved for public release; distribution unlimited.

17. DISTRIBUTION STATEMENT (of the abstract entered in Block 20, if different from Report)

Same

18. SUPPLEMENTARY NOTES

Institute for Computational Mathematics and Applications
Technical Report No. ICMA 81-31

19. KEY WORDS (Continue on reverse side if necessary and identify by block number)

Vortex merger (coalesence); V-state instability; vortex dynamics;
2D hydrodynamics

20. ABSTRACT (Continue on reverse side if necessary and identify by block number)

We present numerical simulations of the instability, merger, and breaking of two piecewise-constant finite-area-vortex-regions (FAVR's). We use an improved contour dynamical algorithm with node insertion-and-removal to maintain the a priori accuracy. We observe that corotating "V-states" (symmetric steady-state FAVR's) are unstable when properly perturbed if their centroid-effective radius, x/R, is < 1.6, thereby verifying an estimate of Saffman and Szeto.

DD FORM 1 JAN 73 1473 EDITION OF 1 NOV 65 IS OBSOLETE
S/N 0102-LF-014-6601

Unclassified
SECURITY CLASSIFICATION OF THIS PAGE (When Data Entered)

(7)

Technical Report ICMA-81-31

EVOLUTION AND MERGER OF ISOLATED VORTEX STRUCTURES

BY

Edward A. Overman, II and Norman J. Zabusky

Institute for Computational Mathematics and Applications
Department of Mathematics and Statistics
University of Pittsburgh, Pittsburgh, PA 15261

82 03 25 151

EVOLUTION AND MERGER OF ISOLATED VORTEX STRUCTURES

Edward A. Overman, II, and Norman J. Zabusky

Institute for Computational Mathematics and Applications
Department of Mathematics and Statistics
University of Pittsburgh, Pittsburgh, PA 15261

ABSTRACT

We present numerical simulations of the instability, merger, and breaking of two piecewise-constant finite-area-vortex-regions (FAVR's). We use an improved contour dynamical algorithm with node insertion-and-removal to maintain the a priori accuracy. We observe that corotating "V-states" (symmetric steady-state FAVR's) are unstable when properly perturbed if their centroid-effective radius ratio, $\bar{x}/R$, is < 1.6, thereby verifying an estimate of Saffman and Szeto. This causes the FAVR's to approach at an exponential rate, merge and reform into a stable perturbed elliptical structure with filamentary arms (to conserve angular momentum). For larger $\bar{x}/R$ ratios, we observe regular perimeter oscillations and thereby obtain estimates of [illegible]-frequency of the perturbed stable V-states. When regions of different vorticity density merge, the larger-density region is eventually entrained within the smaller-density region. These simulations elucidate the self-consistent close interactions of isolated vortex regions in two-dimensional high Reynolds numbers flows.

PACS 47.20.+m, 47.30.+s, 47.25.-c

I. INTRODUCTION

The growth or spread of free shear layers or mixing layers at high Reynolds number has been known for some time. In recent years, careful experiments of Freymuth,[1] Winant and Browand,[2] and Roshko[3] have shown that the initial stages of this growth resulted from the process of "merger" ("pairing" or "coalesence") of like-signed regions of vorticity. This process was clearly observed in 1973 by Christiansen and Zabusky[4] in numerical simulations of the Euler equations with "wake-like" initial conditions. For certain parameters, they observed that two oppositely-signed staggered rows of isolated regions of vorticity were unstable. Eventually like-signed regions merged. They indicated that this process was probably first documented by Taneda[5] in data from experiments on far-wakes behind bluff bodies.

The merger process had already been found numerically by Christiansen and Roberts[6] with a vortex-in-cell code and also by Zabusky, Hughes and Roberts[7] with an early contour dynamics (CD) code. In both "inviscid" studies they began with two FAVR's (piecewise-constant finite-area-vorticity-regions) with circular boundaries.

In the present paper, we present computations with an improved CD code which show that the inviscid merger process may also be conveniently viewed as the long-time behavior of the evolution of an instability of perturbed steady-state corotating "V-states". These states are symmetric FAVR's whose boundaries were determined by Saffman and Szeto[8] and Landau and Zabusky[9] by solving numerically nonlinear integral equations that correspond to the time-independent Euler equations in two dimensions. We also examine the merger of circular FAVR's with each other and with point vortices and indicate the relevance of this process to simulations of high Reynolds number

two-dimensional turbulence. The improvement in the CD code results from the ability to control the truncation error by inserting and removing contour nodes.

Sec. II describes the V-states, the improved CD code and the diagnostics used. Sec. III gives a quantitative account of the merger process of rotating V-states. Sec. IV describes the merger of circular FAVR's. Sec. V concludes with a discussion of the relevance of two-FAVR merger to simulations of two-dimensional turbulent-like motions.

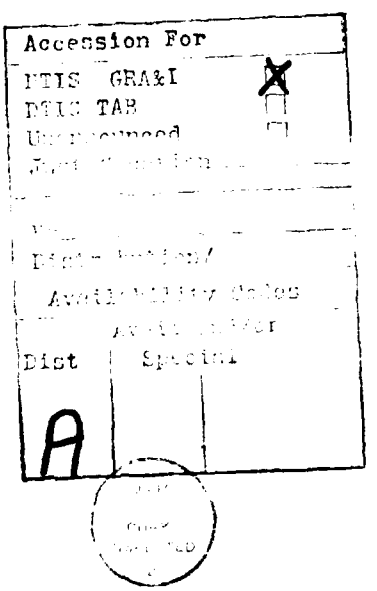

II. EULER EQUATIONS, ROTATING V-STATES, CONTOUR DYNAMICAL ALGORITHM AND DIAGNOSTICS

The Euler equations in two space dimensions can be written in vorticity-stream function form as

$$\omega_t + u\omega_x + v\omega_y = 0, \quad \Delta\psi \equiv \psi_{xx} + \psi_{yy} = -\omega, \tag{1a,b}$$

where

$$u = \psi_y, \quad v = -\psi_x. \tag{1c}$$

If the vorticity is composed of a set of piecewise-constant finite-area-vortex-regions (or FAVR's), that is, each member of the set is a characteristic function χ_i of magnitude ω_i and boundary Γ_i, or $\omega(x,y,t) = \sum_i \omega_i \chi_i(x,y,t)$, then

$$\psi(x,y) = -(2\pi)^{-1} \sum_i \iint_{\mathbb{R}^2} \omega_i \chi_i G(x-\xi, y-\eta)d\xi d\eta, \tag{2}$$

where we use the two-dimensional Green's function

$$G = (1/2)\log[(x-\xi)^2 + (y-\eta)^2] = (1/2)\log r^2 \tag{3}$$

for flow in an unbounded domain. Eq. (1a) says that every point of the fluid including the boundary is convected with the flow. The evolution equation for boundary points (x,y) is the area-preserving mapping

$$(x_t,y_t) \equiv (u(x,y,t),v(x,y,t)) = (2\pi)^{-1} \sum_i \omega_i \int_{\Gamma_i} \log r(d\xi,d\eta). \tag{4}$$

We have used Green's theorem to replace the area integral over the domain of χ_i by the line integral over its boundary, Γ_i, thus reducing the dimension by one.

It is well known[10] that two point (singular) vortices of like circulation Γ and separation $2\bar{x}$ rotate about one another with angular velocity

$$\Omega^* = \Gamma/4\pi\bar{x}^2.$$

In the spirit of desingularization introduced by Deem and Zabusky,[11] one may seek symmetric uniformly rotating doubly-connected regions of finite-area and piecewise-constant vorticity. That is, we apply the boundary condition

$$\underline{n} \cdot \underline{v}_{particle} = \underline{n} \cdot \underline{v}_{boundary} \tag{5}$$

or

$$\partial_s \psi = \Omega r(dr/ds) = 0 \tag{6}$$

where s is the arc length and integrate once to obtain

$$\psi(x,y) + \frac{1}{2}\Omega\,(x^2 + y^2) = c_i, \quad (x,y) \in \Gamma_i, \tag{7}$$

where $i = 1,2$ corresponds to the contours, and ψ is obtained from (2) as a line integral over both contours. Since the location of the boundary is unknown, Eq. (7) is a nonlinear integral equation. It has been solved by Saffman and Szeto[8] and Landau and Zabusky[9] by different numerical iterative procedures. Results from the latter that we call "V-states" are illustrated in Fig. 1.

The numbers on the figure refer to Table 1, which is excerpted from

Table 3 in Reference 9. Included are: x_2, the distance from the center of rotation to the closest contour point; α, the aspect ratio = maximum vertical diameter/$(1-x_2)$; A, the area within one contour; $R = (A/\pi)^{1/2}$, the effective "radius" of a contour; P, the perimeter of a contour; $\bar{x}$, the distance between the center of area and the center of rotation; Ω, the angular velocity of the V-state (the bifurcation parameter); Ω/A, the normalized angular velocity; and $\Omega^* = A/4\pi\bar{x}^2$, the angular velocity of a pair of point vortices of circulation A and separation distance $2\bar{x}$. For our V-state dynamical simulations we used state No. 8, which has $x_2 = 0.1$ or $(\bar{x}/R) = 1.6026$. Note that Saffman and Szeto[8] used Kelvin's ideas on the exchange of stability and showed with numerical calculations that V-states with $(\bar{x}/R) < 1.58$ are unstable.

The contour dynamics algorithm is obtained by discretizing Eq. (4),[7] i.e.,

$$(\dot{x}_m,\dot{y}_m) = \sum_i \omega_i \sum_{n=1}^{N_i} \Delta u_{m,n;i}\,(\cos\theta_{n;i}, \sin\theta_{n;i}) \tag{8}$$

where the i-sum is over all contours and for convenience the i label is suppressed below. We have assumed that nodes n and n+1 are connected by a straight line-segment of length h_n and angle θ_n (from node n to n+1). We carry out exactly the integration in Eq. (4) and obtain

$$\Delta u_{m,n} = \frac{h_n}{2\pi}\left[(1+A_n)\ln r_{m,n+1} - A_n \ln r_{m,n} - 1 + B_n \arctan(2B_n/C_n) + \pi|B_n|\,H(-C_n)\right] \tag{9}$$

where $r_{m,n}$ is the straight line distance between nodes m and n,

$$A_n = \frac{(x_n-x_m)(x_{n+1}-x_n) + (y_n-y_m)(y_{n+1}-y_n)}{h_n^2},$$

$$B_n = \frac{(x_n - x_m)(y_{n+1} - y_n) - (y_n - y_m)(x_{n+1} - x_n)}{h_n^2},$$

$$C_n = \frac{r_{m,n}^2 + r_{m,n+1}^2}{h_n^2} - 1,$$

and H is the Heaviside step function, i.e.,

$$H(z) = \begin{cases} 1 & \text{if } z > 0 \\ 0 & \text{if } z < 0 \end{cases}.$$

If $n = m$, Eq. (9) simplifies to

$$\Delta u_{m,m} = \frac{h_n}{2\pi} [\ln r_{m,m+1} - 1],$$

since $A_m = B_m = 0$, while if $n = m - 1$

$$\Delta u_{m,m-1} = \frac{h_n}{2\pi} [\ln r_{m,m-1} - 1],$$

since $A_{m-1} = -1$ and $B_{m-1} = 0$. Eq. (9) differs from the previously given formula (Ref. 7, Eq. 18) in the last term. This term appears only when $C_n < 0$, or, equivalently, when the angle between the lines from node m to node n and from node m to node $n+1 > \pi/2$. As discussed below, the node insertion-and-removal algorithm will only allow this to happen if the distance between different contours or between different parts of the same contours is less than h_{min}, the minimum allowed distance between <u>adjacent</u> nodes.

The velocities in (8) are used to move the contour node (x_m, y_m) with an Euler predictor and a trapezoidal corrector algorithm. The time step Δt is determined by the maximum change in area (or angular momentum) to be

allowed per unit time. (Since we are solving a Lagrangian system of equations, we do not have a Courant condition to determine the time step.) As shown in the Appendix, the relative change in area of a circular FAVR in one unit of time is

$$\Delta A(1)/A(0) \equiv \frac{A(1) - A(0)}{A(0)} \approx \frac{1}{4} \left| d\underset{\sim}{V}(0)/ds \right|^4 (\Delta t)^3, \tag{10}$$

where $A(t)$ is the area at time t and $\underset{\sim}{V}(0)$ is the velocity of particles on the contour at $t = 0$. Thus,

$$\Delta t = (4\ \Delta A(1)/A(0))^{1/3} \left| d\underset{\sim}{V}(0)/ds \right|^{-4/3}. \tag{11}$$

For <u>arbitrary</u> contours our algorithm chooses Δt analogous to (11), namely

$$\Delta t = \left(4\ \frac{\Delta A(1)}{A(0)} \right)^{1/3} \left(\max_i \left| \frac{d\underset{\sim}{V}_i(0)}{ds} \right| \right)^{-4/3}, \tag{12}$$

where the maximum is over all the nodes on all the contours. In all the runs shown here $\Delta A(1)/A(0) = 0.84375 \times 10^{-6}$ and Δt is readjusted every 20 time steps. We find that $.015 \leq \Delta t \leq .02$ for all the runs.

In the <u>improved</u> node insertion-and-removal algorithm we insert and remove nodes using both local[12] and global adaptive methods. Locally, we attempt to set the internodal distance ℓ_k to

$$c_1/|\kappa_k| \tag{13}$$

which is inversely proportional to the local curvature, but we require it to satisfy two constraints

$$h_{max}^{(g)} \geq h_k \geq h_{min} \tag{14a}$$

and

$$(1-r)h_{k-1} \leq h_k \leq (1+r)h_{k-1}. \tag{14b}$$

In all the runs $c_1 = 0.1$ (which places $\sim 20\pi$ nodes on a circle of unit radius), $h_{min} = 0.01$ and $r = 0.3$. Globally, we choose $h_{max}^{(g)}$ to take into account the possibility that one part of a contour may approach another part or that two contours may approach each other. This is done by setting

$$h_{max}^{(g)} = \max\{\min[h_{max}, c_2\, d_{min}],\, h_{min}\}, \tag{15}$$

where d_{min}, obtained by a search algorithm, is the minimum distance from node k to a point on a neighboring contour or a "nonadjacent" point on the same contour. That is, $h_{max}^{(g)}$ will usually be the minimum of h_{max}, the maximum allowed distance between nodes, and $c_2\, d_{min}$. However, when contours approach, we may have $c_2\, d_{min} < h_{min}$. To avoid this occurrence we have included in (15) the requirement that $h_{max}^{(g)} > h_{min}$. (In all our runs $h_{max} = 0.20$ and $c_2 = 0.50$.)

As diagnostics we monitor the perimeter, P, area, A, (a quantity conserved in the continuum representation) and contour curvature, $\kappa(s) = x_s y_{ss} - x_{ss} y_s$. The origin $s = 0$ of these curvature plots (e.g., Fig. 3b) corresponds to the point on the contour which at $t = 0$ is farthest from the origin and which is advected by (8). This point is designated with a triangle in the physical (x,y) plane. The vertical

scale has a geometric variation $(1^2, 2^2, 3^2, 4^2, 5^2)$ and the curves are "clipped" at $\pm 5^2$. The curvature is computed numerically by differentiating a periodic cubic spline that is fit to the nodes as described in Reference 12, Appendix C. If contours "sharpen" and "break", as observed below, this differentiation can give rise to small-scale oscillations because the cubic spline has difficulty fitting such distributions. These oscillations do not affect our velocities since the curvature is not used in (8).

III. DYNAMICAL EVOLUTION OF PERTURBED ROTATING V-STATES

In case 1.1 the state is "unperturbed", that is, only numerical processes introduce perturbations. In cases 1.2 to 1.6 we examine symmetric perturbations and in case 1.7 we examine an asymmetric perturbation. Parameters for runs in this section are given in Table 2. All contours at $t = 0$ were represented by 72 nodes.

We establish the stationarity of the unperturbed V-state in case 1.1. We let our algorithm evolve state No. 8 up to $T_F = 125$, slightly more than two periods of rotation. In Fig. 2 we show the area change $[\Delta A/A \equiv (A(t) - A(0))/A(0)]$, perimeter change $[\Delta P/P \equiv (P(t) - P(0))/P(0)]$, change in the distance between the center of area and the center of rotation $\bar{x}[\Delta\bar{x}/\bar{x} \equiv (\bar{x}(t) - \bar{x}(0))/\bar{x}(0)]$, and maximum curvature change $[\Delta\kappa/\kappa = (\max|\kappa(t)| - \max|\kappa(0)|)/\max|\kappa(0)|]$. The algorithm kept the number of nodes constant at 72. The linear variation in area change, 0.0458% per period (61.19), following a small negative transient is due to truncation errors, as described above. The perimeter change exhibits an oscillation on a monotonically increasing background that is associated with the area change. The amplitude of the oscillation is a factor of 5 smaller than $h_{min} = 0.01$. The period of the oscillation, 40.6, is 66% of the rotation period. This is an indication of the period of the lowest eigenvalue of small amplitude (linear) perturbations to V-state No. 8. The change in $\bar{x}$ is 180° out of phase with the P change and has the same period. There is a very slow monotonic <u>outward</u> movement of each contour, most likely a numerical artifact. The lack of an inward drift indicates that V-state No. 8 is stable. The maximum curvature change shows an approximate 5% peak-to-peak variation with the same period. The spiky behavior is presently unexplained but, no doubt, due to the cubic spline representation.

Thus, we conclude that numerical processes weakly excite internal degrees of freedom of the V-state and also induce a small but monotonically increasing area or circulation change.

In case 1.2 we introduce a symmetric outward perturbation. That is, we displace each contour outward by 0.02 or increase $\bar{x}$ from 0.5692 to 0.5892 or $(\bar{x}/R)$ from 1.6027 to 1.6590. The duration of the run is 163. The period of rotation as determined from Fig. 3 is 68 (= 163.0/2.4), an increase of 6.3 or 10% over the previous case. This period can be understood if we assume that this state corresponds to a perturbed V-state between No. 7 and No. 8 in Table 1. The maximum and minimum $\bar{x}$ for this state are 0.593 and 0.589. The average of 0.591 is 44% of the way from No. 7 to No. 8. Interpolating Ω/A we find for this state that Ω = .0941 so that the period is 66.8, close to the observed value. Note the regular behavior of the curvature in the sequence in panel b.

Diagnostics are given in Fig. 4. The area change in Fig. 4 shows a small oscillation imposed on a linear variation of smaller magnitude than in case 1.1. The oscillations are more clearly seen in the remaining diagnostics of Fig. 4. The period is 26 or 38% of 68. It is unclear whether this is the lowest or next-lowest eigenvalue associated with perturbations to the contour of the appropriate V-state. The perimeter and $\bar{x}$ deviation show no apparent monotonic behavior. Note that the perimeter, $\bar{x}$ and curvature changes are a factor of 10 larger than in case 1.1. The negative perimeter and curvature changes are indications that the initial condition can be considered a "sharpened" perturbation of an initial V-state which has an $\bar{x}(0)$ larger than that corresponding to state No. 8. This argument supports the calculation of the increase in period given above. Note that a node on the contour makes three full revolutions during 50 units of time

or, approximately one revolution per (1/4) period.

In case 1.3 we seek an unstable regime and displace both contours inward by 0.005 or decrease $\bar{x}$ from 0.5692 to 0.5642 or $(\bar{x}/R)$ from 1.6027 to 1.5886. We obtain the gradual merger for $0 \leq t \leq 32.0$ shown in Fig. 5 with diagnostics in Fig. 6. Note how well the algorithm allows the contours to "slide" close to one another. The maximum curvature grows as they approach. There are two oscillatory regions at $t = 30.0$ in Fig. 5b where the curvature on the graphs is limited to $\pm 5^2$. These are associated with the sharp corners on each contour. The origin of these plots corresponds to the triangle on the (x,y) plots. The growth in perimeter by a factor of 2.19 (= 5.093/2.324) is evident in the increase of the length of the s-axis. The number of nodes grows by a factor of 6.92 (= 498/72). During this time the area change increases by 0.071%, a more rapid increase than in the stable evolutions of cases 1.1 and 1.2. In Fig. 6 we replace the plot of the maximum curvature change with the plot of the logarithm of $\bar{x}$ in order to better show the rate of approach of the two FAVR's. The variation in $\bar{x}$ shows an exponential growth after an initial transient $0 \leq t \leq 4$ in Fig. 6. The straight line fit gives a growth rate $\sigma \approx 0.13$ (in $e^{\sigma t}$).

In case 1.4 we displace both contours inward by 0.02 or decrease $\bar{x}$ from 0.5692 to 0.5492 or $(\bar{x}/R)$ from 1.6027 to 1.5463 and observe a faster merger as shown in Fig. 7 and the diagnostics in Fig. 8. The qualitative features are the same as in case 1.3 except that the time-scale is reduced, that is, the system is more unstable. (Here $\sigma = 0.38$.) As the tips of the contours overlap, the curvature becomes negative and some oscillatory structure again develops locally because of the locally poor fit of the periodic cubic spline. Between $9.0 \leq t \leq 11.0$ we see two sharp minus-to-plus transitions associated with the tips of the two contours. There is also a rapid increase

in nodes from $N = 146$ to $N = 473$ between $14.0 \leq t \leq 18.0$.

In case 1.5 we continue the previous run to longer times. We remove the common boundary at $t = 10$ and smooth the state slightly to obtain a new initial condition whose evolution is shown in Fig. 9. The area of the singly-connected state of Fig. 9 at $t = 10$ is 0.7893, or 0.37% smaller than the corresponding state in Fig. 7 at $t = 10$. The smoothed curvature in Fig. 9b at $t = 10$ is nearly identical to that in Fig. 7b at $t = 10$ in the region enclosed between the arrows above. The slight asymmetry in the negative peaks (arrows below) is an artifact of the cubic spline fit to the contour.

The evolution of Fig. 9 may be considered that of a 6:1 ellipse with a strong symmetrical perturbation.[13] (Results of asymmetrical perturbations to a 3.5:1 ellipse have been given previously.[14]) The indentations fill out as waves propagate about the contour, but the contour "breaks" and symmetrical filamentary arms form and grow in length. At $t = 37.5$ we see the arms tending to pinch near the central region of vorticity (*), and evidence that the arms are beginning to "roll-up" at their ends (**). The latter is more clearly seen in the curvature plots of Fig. 9b ($t = 30$, 35, and 37.5). The inclined arrows point to a negative dip in curvature, the signature for incipient roll-up. Note that the ellipse-like central region has a ratio of axes ≈ 2.8.

In case 1.6 we do not displace the contours but perturb the right FAVR of V-state No. 8 with a "third" harmonic to obtain an asymmetric perturbation. That is, if $\underset{\sim}{R}_{(8)}(s)$ is the position as a function of arc length with respect to the centroid, we obtain the perturbed position $\underset{\sim}{R}$ as

$$\underset{\sim}{R}(s) = \underset{\sim}{R}_{(8)}(s) + (0.005)\cos(6\pi s/P_{(8)})\, \underset{\sim}{e}_n(s), \qquad (16)$$

where $\underset{\sim}{e}_n$ is the outward normal to the unperturbed contour and $P_{(8)}$ is the perimeter of the unperturbed contour. This causes the right contour to have an area $A = 0.4076$ and perimeter $P = 2.357$, 2.85% and 1.33% larger than the left contour, respectively. It also causes the right centroid to be shifted inward to $\bar{x} = 0.5691$ a decrease of 0.02%. We observe merger on a time scale somewhat larger than in case 1.3. The asymmetric nature of the evolution is shown in the diagnostics of Fig. 11.

IV. DYNAMICAL EVOLUTION OF FAVR'S OF VARYING STRENGTH AND AREA

We next present a panorama of cases which illustrates how a change in vorticity density alters the merger process from one of "wrap-around" to one of "entrainment". The parameters and properties of the cases are summarized in Table 3. In cases 2.1 through 2.4 and 2.7 FAVR 1 (left) and 2 (right) are circles, and in cases 2.5 and 2.6 FAVR 1 is a circle and PV 2 is a point vortex. In all cases FAVR 1 is a circle of radius 1, centered at the origin, with vorticity 1. FAVR 2 is a circle of radius r_2 centered at the point $(x_{2c},0)$ with vorticity ω_2 and circulation Γ_2 and PV 2 is a point vortex, also centered at $(x_{2c},0)$, with circulation Γ_2.

In cases 2.1 to 2.3, Fig. 12a,b,c, $r_2 = 0.2$ and $\omega_2 = 2.5$ so that the ratio of the circulations of FAVR 1 to FAVR 2 is 10:1. In case 2.1, panel a, the separation is sufficient, $x_{2c} = 2.0$, so no merger occurs. We see mutual interactions that lead to elliptical and higher harmonic deformations and near-recurrence to initial states. In case 2.2, panel b, we decrease the separation distance, $x_{2c} = 1.8$, and obtain merger. Note that as the smaller region slides along the larger, it tends to "draw-out" the vorticity in a "step". The "angle" of the step (included between the dashed lines) increases with time, indicating that entrainment is occurring. This results because the smaller region has the larger vorticity density. We conjecture that eventually region 1 will be wrapped around region 2. In case 2.3, panel c, we decrease the separation distance further, $x_{2c} = 1.6$, and see similar quantitative features to those obtained in case 2.2, except that the time scale has decreased to $8/19 \sim 0.42$.

In case 2.4, Fig. 12d, $r_2 = (.1)^{1/2}$ and $\omega_2 = 1.0$ so the ratio of circulations is still 10:1. $x_{2c} = 1.8$ as in case 2.2. There is a tendency

toward "wrap-around". FAVR 2 increases in perimeter from 1.9861 to 9.7239 and the number of nodes increases from 63 to 240 at $t = 12$. Also the center of area (the "x") of FAVR 2 leaves the inside of the region between $8 < t < 9$ as it elongates and curves and approaches the first FAVR.

In cases 2.5 and 2.6, Fig. 13a,b, we "singularize" the right FAVR and keep the ratio of circulations at 10:1. The point vortex is represented by a point surrounded by a square. In case 2.5, panel a, they are sufficiently separated, $x_{2c} = 2.0$, so no merger occurs as in case 2.1, Fig. 12a. We have run this for a long time ($t_F = 328$) and show somewhat more than one full rotation of the point about the FAVR near the end of the run. In case 2.6, panel b, the initial distance of separation is decreased, $x_{2c} = 1.8$, and merger by "entrainment" occurs, which has a qualitatively different character than case 2.2, Fig. 12b. In case 2.7, panel c, the right vortex is a FAVR with $r_2 = 0.2$ and $\omega_2 = 7.854$ so the ratio of circulations of FAVR 1 to FAVR 2 is 3.183:1. The initial distance of separation is the same as in case 2.5 where no merger occurs, i.e., $x_{2c} = 2.0$. We observe qualitatively similar merger by entrainment proceeding at a faster time-scale than in case 2.6. Thus, decreasing the circulation ratios (by increasing the vorticity density of the smaller) changes a stable system (case 2.1) into an unstable system (case 2.7). Furthermore, the qualitative nature of the entrainment of regions of larger vorticity density is independent of whether they are point vortices or small FAVR's.

V. CONCLUSIONS

We have applied an improved contour dynamical algorithm to study the merger process. By using an adaptive node insertion-and-removal algorithm we control the magnitude of the truncation error. We present diagnostics including a "microscopic" view of curvature vs arc length of contours.

We observe that if a stable V-state or a stable perturbed V-state is displaced inward across the point of "exchange of stability" we will have merger. Furthermore, the larger the inward perturbation the more unstable is the resulting system or the larger the real part of the dominant eigenvalue σ ($e^{\sigma t}$).

If two states with different vorticity density merge, the region of larger vorticity density will be entrained within the region of smaller vorticity density. Physically we expect this, for the Rayleigh stability criteria states that localized vortex regions with negative vorticity gradients and no inflection points are stable. That is, the merger process continues until something like a stable-perturbed state is obtained. We guess that these states are "near" to the desingularized doubly-connected stationary states conjectured by Landau and Zabusky.[9]

The "breaking" of evolving merged vortex states was already observed by Christiansen and Zabusky[4] in the qualitative simulations of model inviscid wakes. The resulting "central" region of vorticity has the form of a stable perturbed elliptical FAVR and the filamentary arms, if properly dissociated ("pinched") from the central region appear to be in the process of slow "roll-up", something one expects from a sheetlike region of vorticity.

There are lessons here for the simulation of two-dimensional environments with turbulent-like motions. Finite-difference or spectral methods are adequate for internal flows or flows with periodic boundary conditions at

moderate Reynolds number. However, for flows at very-high Reynolds number with no-near boundaries (and unbounded domains) the contour dynamical method and the invariant-core vortex (ICV) method, e.g., as proposed by Chorin,[15,16,17] are possible grid-free choices. The former may require two or more nested contours per region to adequately represent realistic continuum vorticity variations. However, the contour dynamical method is more accurate than the ICV method. As shown in Hald [18], the spatial error for the ICV method is $O(N^{-1})$ in the L_2 norm and $O(N^{-1/2})$ in the maximum norm, where N is the number of point vortices used to cover a two-dimensional region. In the contour dynamical model the error is $O((h_n)^2) \approx O(N_c^{-2})$ in the maximum norm, where N_c is the number of nodes on the contours. In both models the number of operations per time step is $O(N^2)$ or $O(N_c^2)$, respectively. The weak approach to the continuum for the ICV method indicates that the intermediate "spectrum" (or scale-sizes) of the turbulent-like processes may be subject to systematic errors at long times if a "reasonable" number of particles are not used.

ACKNOWLEDGEMENTS

This work was supported by ONR Contracts N00014-77-C-0520 and N00014-81-C-0531, Task NR 062-583.

REFERENCES

1. P. Freymuth, On transition in a separated laminar boundary layer. J. Fluid Mech. 25, 683, 1966.
2. C. D. Winant and F. K. Browand, Vortex pairing: the mechanism of turbulent mixing layer growth at moderate Reynolds number. J. Fluid Mech. 63, 237, 1974.
3. A. Roshko, Structure of turbulent shear flows: a new look. AIAA J. 14, 1349, 1976.
4. J. P. Christiansen and N. J. Zabusky, Instability, coalescence and fission of finite area vortex structures. J. Fluid Mech. 61, 219, 1973.
5. S. Taneda, Experimental investigation of the wakes behind cylinders and plates at low Reynolds numbers. J. Phys. Soc. Japan 11, 302, 1956; Oscillations of the wake behind a flat plate parallel to the flow. J. Phys. Soc. Japan 13, 418, 1958; and Downstream development of wakes behind cylinders. J. Phys. Soc. Japan 14, 834, 1959.
6. K. V. Roberts and J. P. Christiansen, Topics in computational fluid dynamics. Computer Phys. Comm. 3 Suppl., 14-32, 1974.
7. N. J. Zabusky, M. Hughes and K. V. Roberts, Contour dynamics for the Euler equation in two dimensions. J. Comp. Phys. 30, 96, 1979.
8. P. G. Saffman and R. Szeto, Equilibrium shapes of a pair of equal uniform vortices. Phys. Fluids 23, 2339, 1980.
9. M. Landau and N. J. Zabusky: Stationary solutions of the Euler equations in two dimensions. Singly- and doubly-connected V-states. Submitted for publication, 1981.
10. G. K. Batchelor: An Introduction to Fluid Dynamics. Cambridge University Press, Sec. 7.3, p. 531, 1970.

REFERENCES (Continued)

11. G. S. Deem and N. J. Zabusky, Vortex waves: stationary V-states, interactions, recurrence and breaking. Phys. Rev. Lett. 40, 859, 1978.

12. N. J. Zabusky and E. A. Overman, II: Regularization of contour dynamical algorithms. J. Comp. Phys., accepted for publication, 1981.

13. A. E. H. Love, On the stability of certain vortex motions. Proc. Lond. Math. Soc. 35 (1), 18-42, 1893.

14. N. J. Zabusky, Recent developments in contour dynamics for the Euler equations. Proceedings of the Conference on Collective Phenomena, Moscow, 1979. New York Academy of Sciences, 1981. Also see M. Landau, The structure and stability of finite area vortex regions of the two dimensional Euler equations. Ph.D. thesis, University of Pittsburgh, 1981.

15. A. J. Chorin, Numerical study of slightly viscous flow. J. Fluid Mech. 57, 785-796, 1973.

16. A. J. Chorin, Vortex sheet approximation of boundary layers. J. Comput. Phys. 27, 428, 1978.

17. F. Milinazzo and P. G. Saffman, J. Comput. Phys. 23, 380-392, 1977 and P. G. Saffman, Reply to comment by A. J. Chorin, J. Comp. Phys. 26, 455-456, 1978.

18. O. H. Hald, Convergence of vortex methods for Euler's equations, II. SIAM J. Numer. Anal. 16, 726, 1979.

APPENDIX: Time step for predictor-corrector algorithm.

For convex figures the predictor-corrector algorithm causes a net area growth which can be controlled by decreasing the time step, Δt, as we now describe. Consider a circular FAVR of radius R_o and vorticity density ω. The speed of a boundary point is

$$V_o = \omega R_o/2. \tag{A1}$$

Thus, the predictor algorithm displaces the point $(R_o,0)$ to $(R_o,V_o\Delta t)$ and the velocity at the point is $V_o(-V_o\Delta t/R_o,1)$. Thus, the corrector algorithm (which averages the velocities) displaces the point $(R_o,0)$ to $(R_o - (V_o\Delta t)^2/2R_o, V_o\Delta t)$. This yields a circle with areas

$$A(\Delta t) = \pi R_o^2 \left[1 + \frac{1}{4}(V_o\Delta t/R_o)^4\right]. \tag{A2}$$

The relative change in area in one unit of time is

$$\frac{A(1) - A(0)}{A(0)} \equiv \frac{\Delta A(1)}{A(0)} \approx \frac{1}{4}\left(\frac{V_o}{R_o}\right)^4 (\Delta t)^3. \tag{A3}$$

We note that for circular FAVR's

$$V/R \equiv |d\underset{\sim}{V}/ds|, \tag{A4}$$

where $\underset{\sim}{V}$ is the velocity of any point on the contour. Eq. (A 4) is the basis for generalizing to a noncircular FAVR.

Table 1. Doubly-connected symmetric rotating V-states (ω_i = 1.0).

N[a]	x_2[b]	α[c]	A	R[d]	P	$\bar{x}$	Ω	Ω/A	Ω^*[e]
1	0.80	0.9943	0.03123	0.09970	0.6265	0.9000	0.003068	.09824	0.003068
3	0.60	0.9685	0.1217	0.1968	1.237	0.8002	0.01513	.1243	0.01512
5	0.40	0.9044	0.2553	0.2851	1.795	0.7015	0.04146	.1624	0.04129
6	0.30	0.8461	0.3244	0.3213	2.030	0.6536	0.06108	.1883	0.06043
7	0.20	0.7597	0.3782	0.3470	2.213	0.6082	0.08344	.2206	0.08139
8	0.10	0.6395	0.3963	0.3552	2.326	0.5692	0.1027	.2591	0.09733
9	0.05	0.5726	0.3864	0.3507	2.357	0.5566	0.1073	.2777	0.09925
10	0.01	0.5342	0.3771	0.3465	2.389	0.5545	0.1074	.2848	0.09760

(a) Odd numbered contours are shown in Fig. 1.

(b) x_2 is the point closest to the origin. All curves are normalized so that the point farthest from the origin is at 1.0.

(c) Aspect ratio, α = maximum vertical diameter / maximum horizontal diameter.

(d) $R = (A/\pi)^{1/2}$

(e) $\Omega^* = A/4\pi\bar{x}^2$

Table 2. Parameters for the dynamical simulation of perturbed V-states.

Case	Figures	Initial Contours	Initial Perturbation
1.1	2	V-state No. 8	None
1.2	3,4	V-state No. 8	Each contour 0.02 outward ($\bar{x}(0) = 0.5892$)
1.3	5,6	V-state No. 8	Each contour 0.005 inward ($\bar{x}(0) = 0.5642$)
1.4	7,8	V-state No. 8	Each contour 0.02 inward ($\bar{x}(0) = 0.5492$)
1.5	9	State in case 1.4 at $t = 10$ with common boundary removed	
1.6	10,11	V-state No. 8	Right contour with "third" harmonic, Eq. (16)

Table 3. Parameters for merger/no-merger runs (in all cases FAVR 1 has center at (0,0), $r_1 = 1$, $\omega_1 = 1$, $\Gamma_1 = 3.142$).

Case	Figure	x_{2c}	r_2	ω_2	Γ_2	t_F	Behavior until t_F
2.1	12a	2.0	0.2	2.5	.3142	38	no merger
2.2	12b	1.8	0.2	2.5	.3142	19	merger
2.3	12c	1.6	0.2	2.5	.3142	10	merger
2.4	12d	1.8	0.3162	1.0	.3142	12	wrap-around
2.5	13a	2.0	0.0	—	.3142	328	no merger
2.6	13b	1.8	0.0	—	.3142	24	merger
2.7	13c	2.0	0.2	7.854	.9870	15.78	merger

FIGURE CAPTIONS

1. Rotating symmetrical V-states. Parameters are given in Table 1.
2. Diagnostics for the unperturbed V-state No. 8, case 1.1.
   a) $\Delta A/A = (A(t) - A(0))/A(0)$;
   b) $\Delta P/P = (P(t) - P(0))/P(0)$;
   c) $\Delta\bar{x}/\bar{x} = (\bar{x}(t) - \bar{x}(0))/\bar{x}(0)$;
   d) $\Delta\kappa/\kappa = (\max|\kappa(t)| - \max|\kappa(0)|)/\max|\kappa(0)|$.
3. Outward perturbed V-state No. 8, case 1.2.
   a) Physical space;
   b) Curvature vs arc length.
4. Diagnostics for the outward perturbed V-state No. 8, case 1.2.
   See Fig. 2 for explanation of panels.
5. Inward perturbed V-state No. 8, case 1.3.
   a) Physical space;
   b) Curvature vs arc length.
6. Diagnostics for the inward perturbed V-state No. 8, case 1.3.
   a) $\Delta A/A = (A(t) - A(0))/A(0)$;
   b) $\Delta P/P = (P(t) - P(0))/P(0)$;
   c) $\Delta\bar{x}/\bar{x} = (\bar{x}(t) - \bar{x}(0))/\bar{x}(0)$;
   d) $\ln|\Delta\bar{x}/\bar{x}| = \ln|(\bar{x}(t) - \bar{x}(0))/\bar{x}(0)|$.
7. Inward perturbed V-state No. 8, case 1.4.
   a) Physical space;
   b) Curvature vs arc length.
8. Diagnostics for the inward perturbed V-state No. 8, case 1.4.
   See Fig. 6 for explanation of panels.
9. Inward perturbed V-state No. 8, case 1.5. Continuation of case 1.4 from $t = 10$, where the common boundary has been removed.

FIGURE CAPTIONS (Continued)

a) Physical space;

b) Curvature vs arc length.

10. Asymmetrically perturbed V-state No. 8, case 1.6.

11. Diagnostics for asymmetrically perturbed V-state No. 8, case 1.6. See Fig. 6 for an explanation of panels.

12. Circular FAVR interactions. FAVR 1 has center at $(0,0)$, $r_1 = 1$, $\omega_1 = 1$, $\Gamma_1 = 3.142$. FAVR 2 has center at $(x_{2c},0)$.

a) Case 2.1, $x_{2c} = 2.0$, $r_2 = 0.2$, $\omega_2 = 2.5$, $\Gamma_2 = .3142$

b) Case 2.2, $x_{2c} = 1.8$, $r_2 = 0.2$, $\omega_2 = 2.5$, $\Gamma_2 = .3142$

c) Case 2.3, $x_{2c} = 1.6$, $r_2 = 0.2$, $\omega_2 = 2.5$, $\Gamma_2 = .3142$

d) Case 2.4, $x_{2c} = 1.8$, $r_2 = 0.3162$, $\omega_2 = 1.0$, $\Gamma_2 = .3142$

13. FAVR-FAVR or FAVR-point vortex interactions. FAVR 1 is as in Fig. 12. Circular FAVR 2 or PV 2 has center at $(x_{2c},0)$.

a) Case 2.5, PV 2, $x_{2c} = 2.0$, $\Gamma_2 = .3142$

b) Case 2.6, PV 2, $x_{2c} = 1.8$, $\Gamma_2 = .3142$

c) Case 2.7, FAVR 2, $x_{2c} = 2.0$, $r_2 = 0.2$, $\omega_2 = 7.854$, $\Gamma_2 = 0.9870$

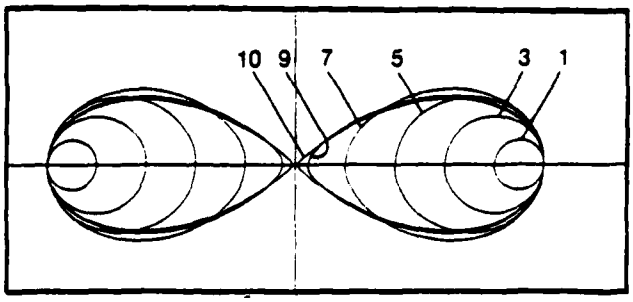
10
9
7
5
3
1

Fig.1

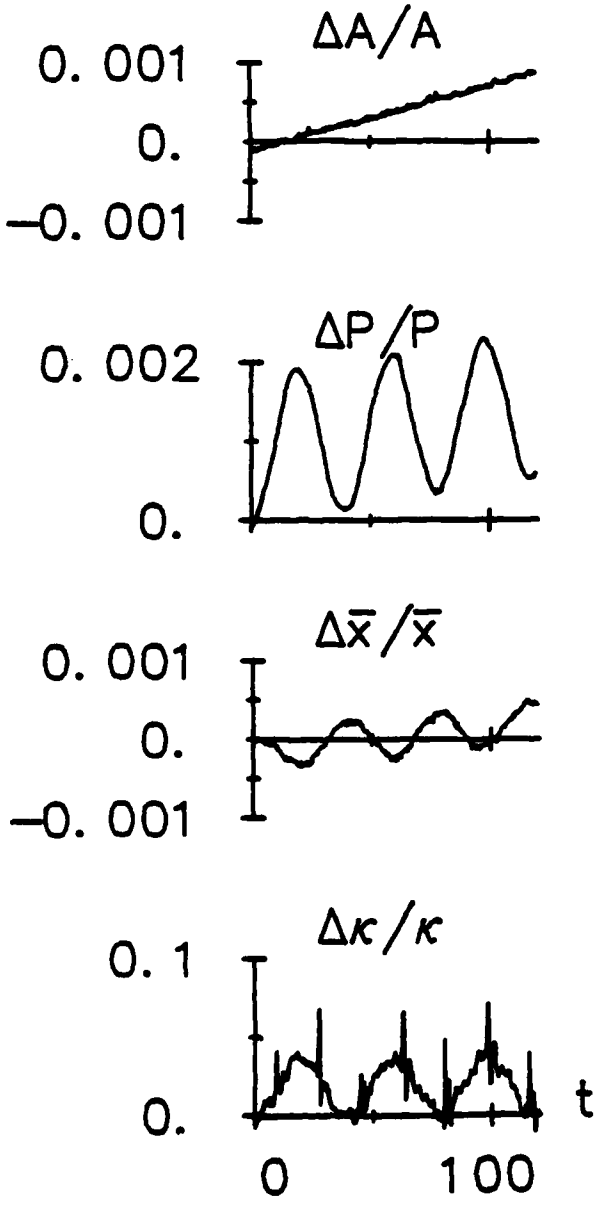
ΔA/A
0. 001
0.
−0. 001
ΔP/P
0. 002
0.
Δx̄/x̄
0. 001
0.
−0. 001
Δκ/κ
0. 1
0.
t
0
100

Fig.2

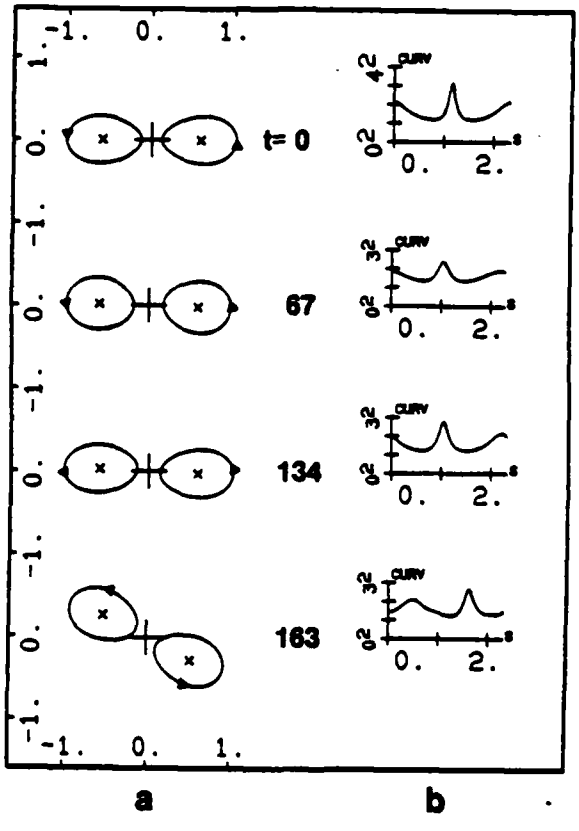

Fig.3

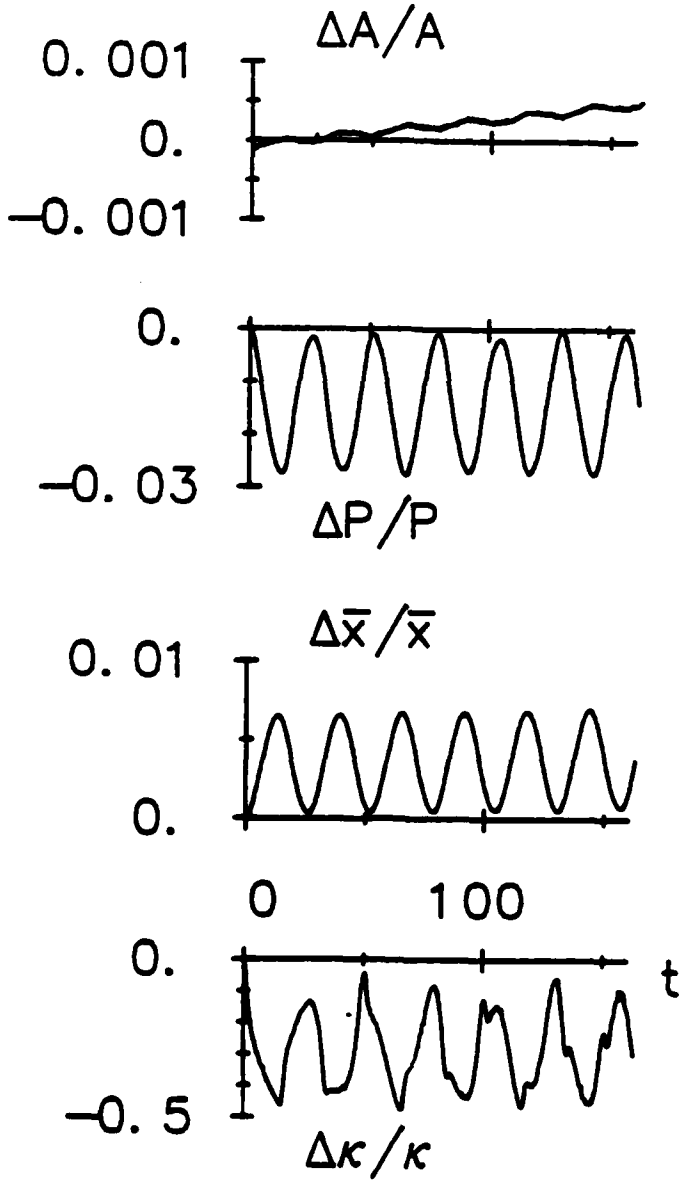

Fig.4

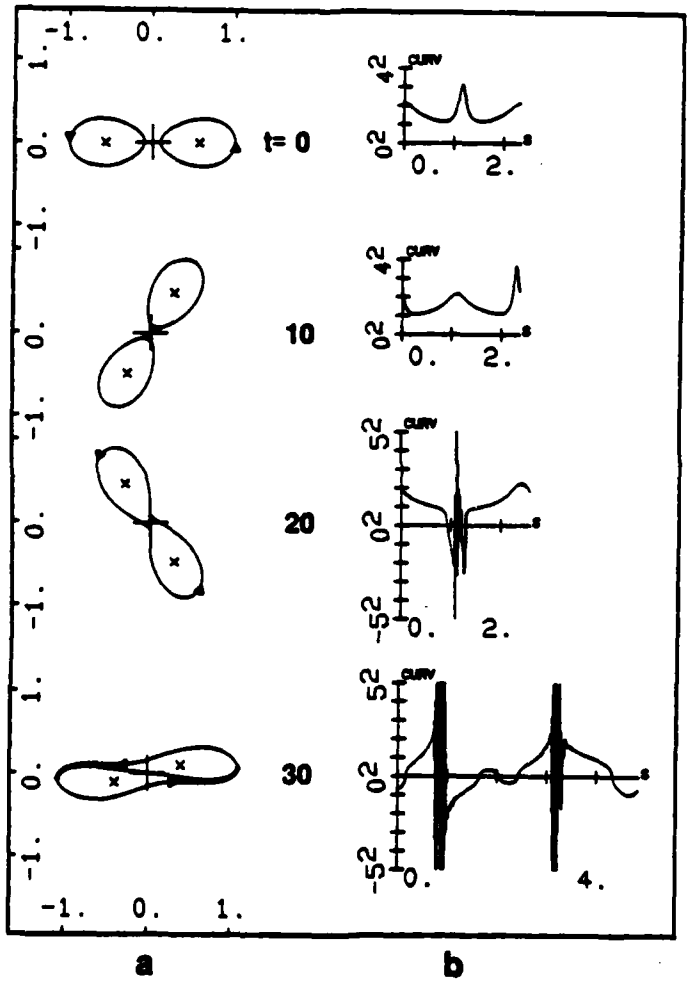

Fig.5

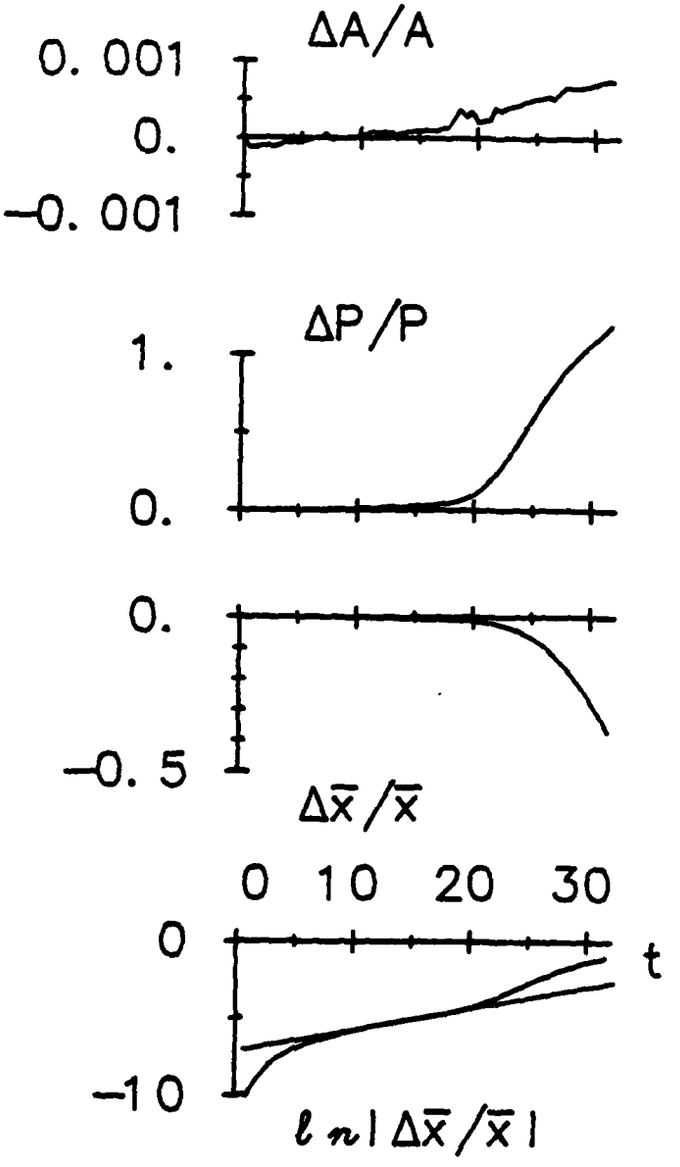

Fig.6

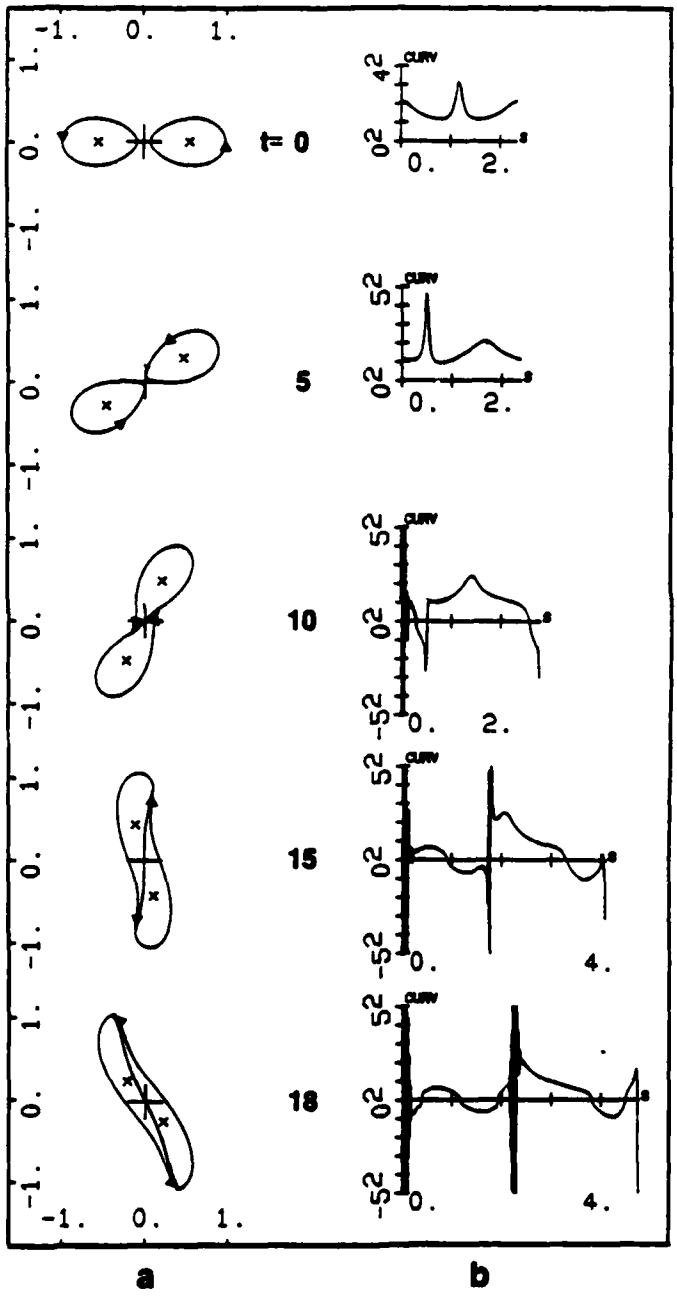

Fig.7

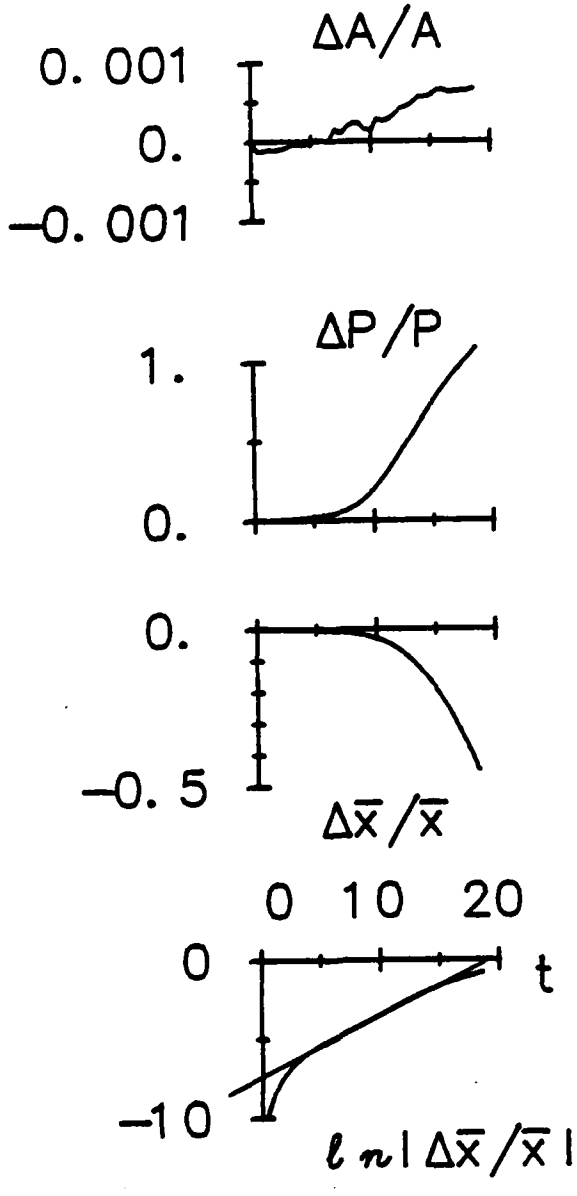

Fig.8

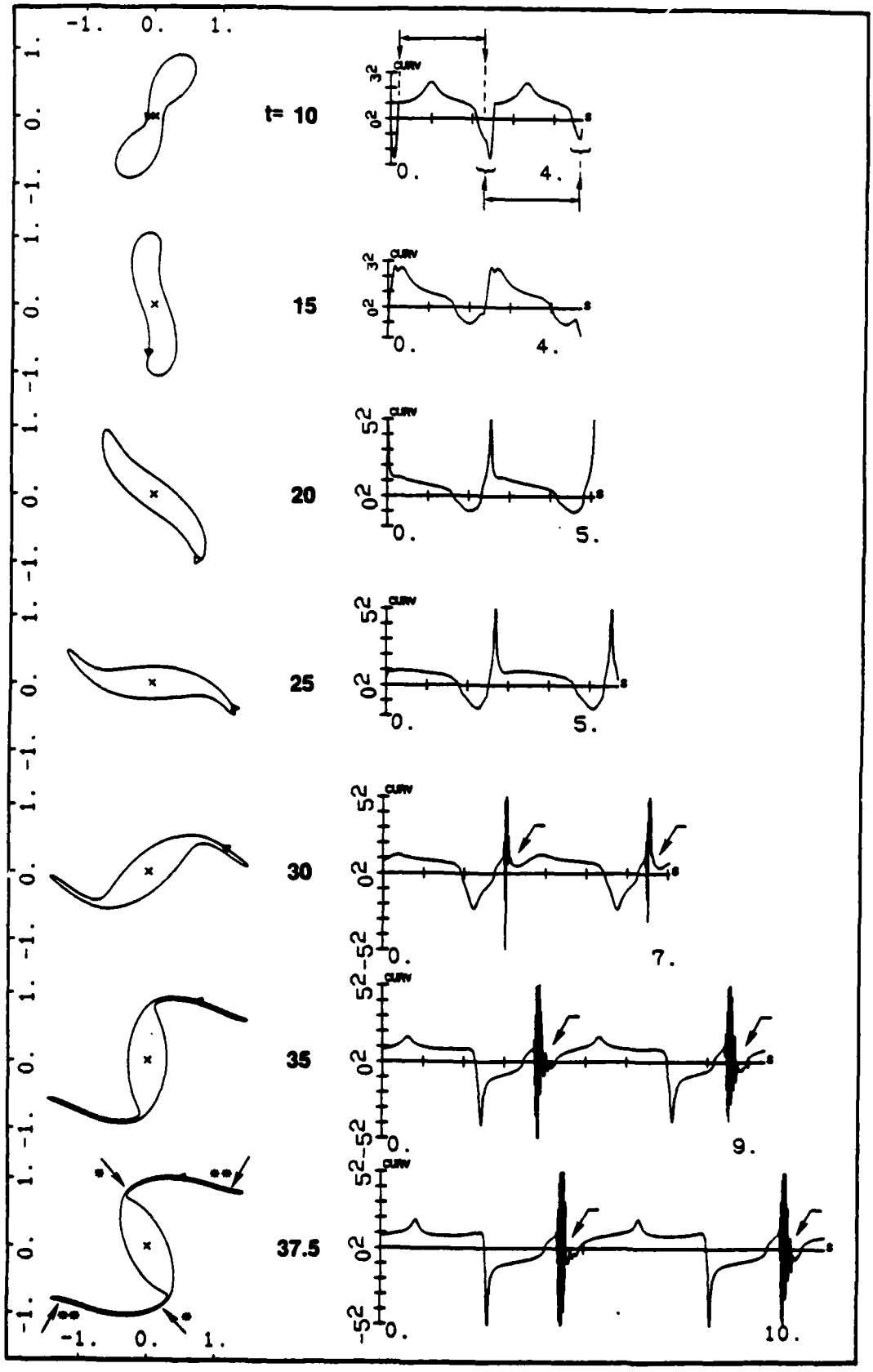

Fig.9

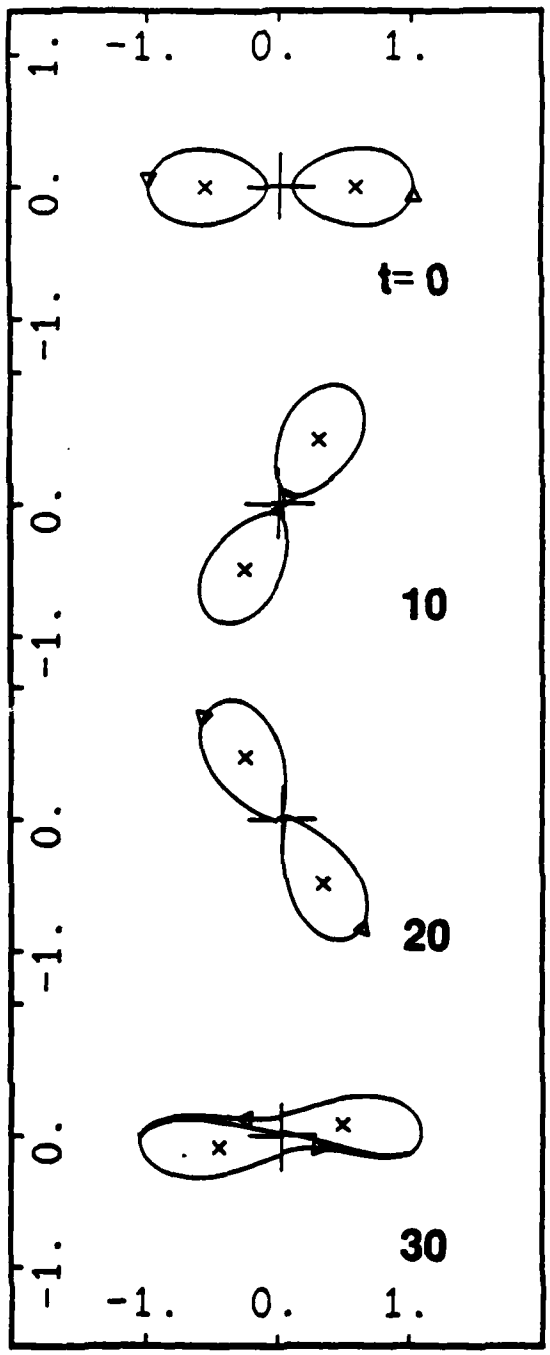

Fig.10

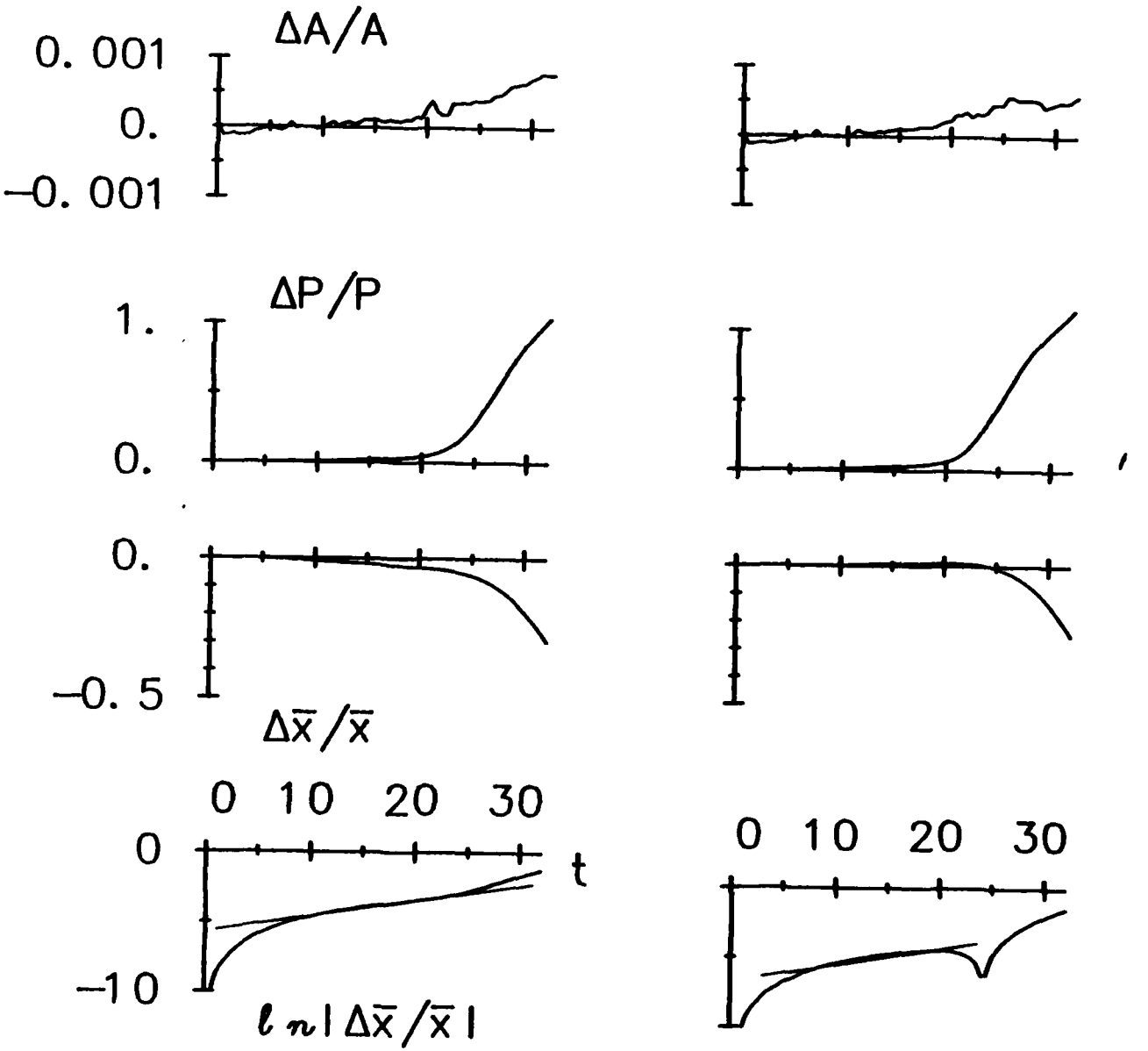

Fig.11

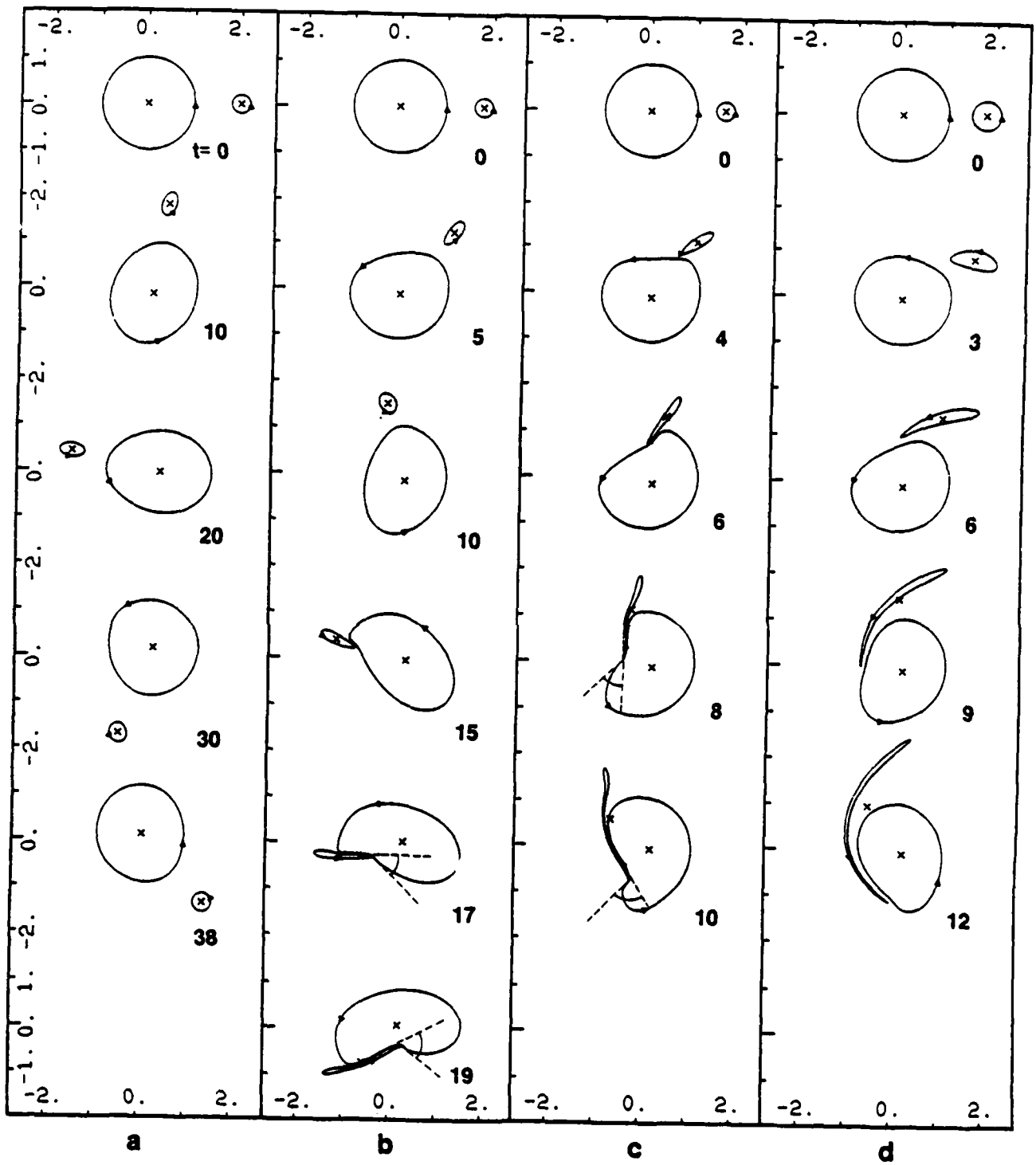

Fig.12

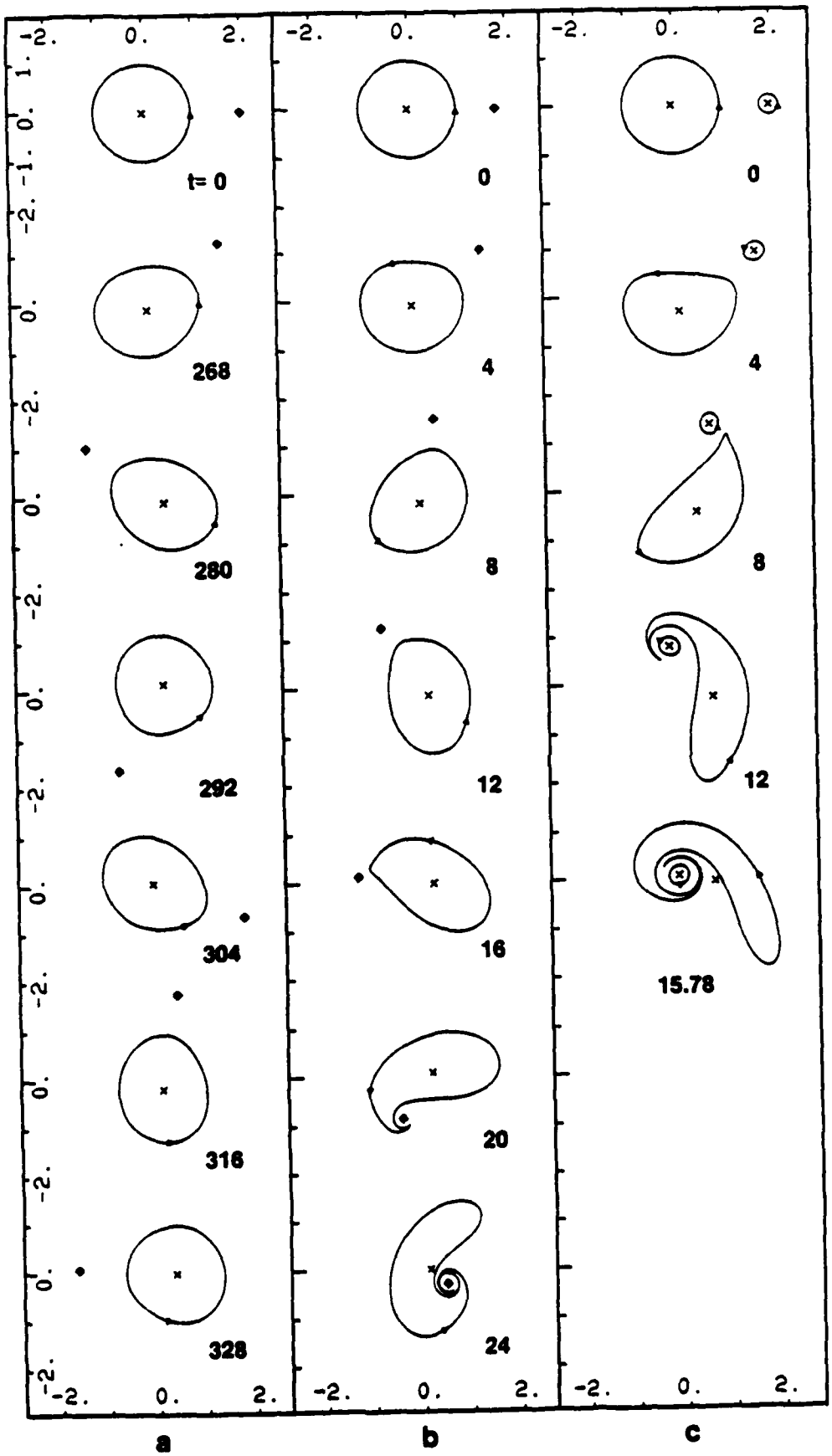

Fig.13

END

DATE
FILMED
4-82

DTIC